Electronic Supporting Information

Constructing layer-by-layer self-assembly MoS$_2$/C nanomaterials by one-step hydrothermal method for catalytic hydrogenation of phenanthrene

Rong Huang,[ab] Chenggong Yang,[ab] Na Ta,[c] Huaijun Ma,[a] Wei Qu,[a] Congxin Wang,[a] Zhendong Pan,[a] Donge Wang*[a] and Zhijian Tian[ac]

[a] Dalian National Laboratory for Clean Energy, Dalian Institute of Chemical Physics, Chinese Academy of Sciences, Dalian, 116023, China
[b] University of Chinese Academy of Sciences, Beijing 100049, China
[c] State Key Laboratory of Catalysis, Dalian Institute of Chemical Physics, Chinese Academy of Sciences, Dalian, 116023, China

Experimental Section

Chemicals. Ammonium paramolybdate ($(NH_4)_6Mo_7O_{24}.4H_2O$), thiourea (CH_4N_2S), and sucrose ($C_{12}H_{22}O_{11}$) were purchased from Tianjin Kermel Chemical Reagent Company. Tridecane and phenanthrene were purchased from Aladdin Industrial Corporation. Chemicals were utilized without further purification.

Synthesis of MoS$_2$ and MoS$_2$/C samples. 0.45 mmol of $(NH_4)_6Mo_7O_{24}.4H_2O$, 32.84 mmol of CH_4N_2S, and 1.30 mmol of sucrose ($C_{12}H_{22}O_{11}$) were dissolved in 60 ml of deionized water. The resulting solution was transferred into a 100 ml Teflon-lined autoclave, and kept at 210 ℃ for 24 h. The products were filtered, washed with distilled water several times, and dried in a vacuum oven at 60 ℃ over night. The obtained sample with C/Mo molar ratio of 5 in the precursor was denoted as MoS$_2$/C, that is, MoS$_2$/C-5. MoS$_2$/C catalysts with C/Mo molar ratios from 0.7 to 27 in the precursor were also synthesized and denoted as MoS$_2$/C-X. For comparison, the MoS$_2$ sample was prepared by a similar procedure in the absence of sucrose. The detailed synthesized conditions are summarized and listed in Table S1.

Table S1. The preparation conditions for MoS$_2$ and MoS$_2$/C samples in this work.

Samples	Mo sources/mmol	S sources/mmol	C sources/mmol
MoS$_2$	0.45	32.84	\
MoS$_2$/C(MoS$_2$/C-5)	0.45	32.84	1.30
MoS$_2$/C-0.7	0.45	32.84	0.182
MoS$_2$/C-1	0.45	32.84	0.260
MoS$_2$/C-7	0.45	32.84	1.82
MoS$_2$/C-10	0.45	32.84	2.60
MoS$_2$/C-15	0.45	32.84	3.90
MoS$_2$/C-27	0.45	32.84	7.02

Characterizations of MoS$_2$ and MoS$_2$/C samples. The X-ray diffraction (XRD) patterns were acquired on a PANalytical X'Pert Pro X-ray diffractometer equipped with nickel-filtered Cu Ka radiation (λ=0.15418 nm) with 40 kV and 40 mA. Raman spectra were measured on a Renishaw inVia Raman spectrometer with 532 nm excitation line. The amounts of C, H, N, S in samples were analyzed using a Flash 2000 organic elemental analyzer from Thermo Scientific, and the amounts of Mo in samples were analyzed on a Optima 7300DV ICP-OES. The scanning electron

microscopy (SEM) and high-resolution transmission electron microscopy (HRTEM) images of samples were respectively taken from a JSM 7800F microscope and a JEM 2100 microscope. The scanning transmission electron microscopy (STEM) images and line-scan elemental distributions were obtained on a JEM F200 microscope with X-ray energy-dispersive spectroscopy. X-ray photoelectron spectroscopy (XPS) measurements were carried out on a Thermo Fisher Scientific ESCALAB 250Xi spectrometer with monochromatized Al Kα excitation, and the C 1s peak (284.8 eV) was used as reference.

Table S2. The elemental analysis for MoS_2 and MoS_2/C samples.

| Samples	C^a wt.%	H^a wt.%	N^a wt.%	S^a wt.%	Mo^b wt.%	C/Mo mol/mol	S/Mo mol/mol
MoS_2	0	0.93	2.14	35.49	51.62	0	2.06
MoS_2/C	7.71	1.43	3.01	29.04	41.41	1.49	2.10

a-analyzed by CHNS; b-analyzed by ICP-OES.

Catalytic activities of MoS_2 and MoS_2/C samples. The catalytic activities of catalysts were evaluated by hydrogenation of phenanthrene (PH) in slurry bed reactor as our previous work. Catalytic activity for PH hydrogenation was evaluated in a 100 ml Parr high pressure micro-reactor. 30.0 g of tridecane solvent, 3.0 g of PH, and a certain amount of catalyst with 0.075g of catalytic active MoS_2 were put into the micro-reactor. The dosage of catalyst was calculated according to the results of elemental analysis, in which molybdenum was 45 mg. Hydrogen was purged into the micro-reactor three times to exchange the air in the reaction system, and subsequently, the micro-reactor was charged with H_2 to an initial pressure of 8.0 MPa at room temperature. Hydrogenation reaction was performed at 350 ℃ with a stirring rate of 300 r.p.m.. After the reaction was maintained for 4 h, the micro-reactor was naturally cooled down. The liquid products were obtained by filtering the catalyst with filter membrane. The liquid products were identified with Agilent 7890B-5977A GC-MS, and quantitatively analyzed with a gas chromatograph (Agilent 7890A with a FID detector and a HP-5 column).

With polycondensed ring aromatic hydrocarbons, the first-ring hydrogenation into preliminary hydrogenation product has been observed to be most favored kinetically.

The rates of hydrogenation of subsequent rings tend to become lower and more difficult, and hydrogenation of the last ring into deep hydrogenation product proceeds with considerable difficulty compared with the initial hydrogenation steps.[1] The products of PH hydrogenation are mainly PH derivatives including PH2, PH4, PH8, and PH14. The reaction pathway of PH hydrogenation was given in Scheme S1.
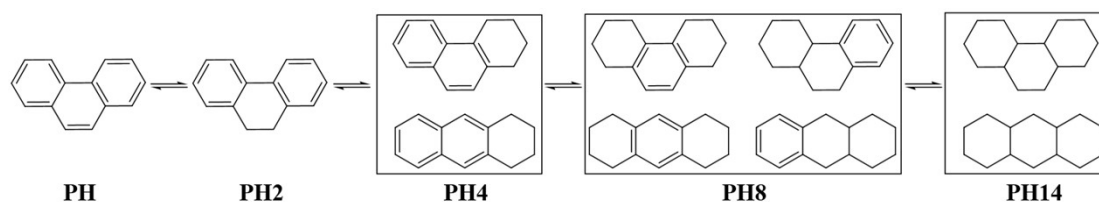
Scheme S1. Reaction pathways for phenanthrene hydrogenation using MoS_2 catalysts.

The PH conversion (Conv.), PH hydrogenation percent (HP), and product selectivity ($Sel.$) were calculated as follows.

The hydrogenation product selectivity (Sel.) to PHx is calculated with Eq. (1).

$$Sel._{(PHx)}(mol\%) = \frac{AT(PHx) \times 100\%}{AT(PH2) + AT(PH4) + AT(PH8) + AT(PH14)} \quad (1)$$

AT(PHx) means the molar of PHx.

The conversion (Conv.) is calculated with Eq. (2).

$$Conv.(\%) = \frac{[PH]_0 - [PH]}{[PH]_0} \times 100\% \quad (2)$$

$[PH]_0$ means the initial concentration of PH, and $[PH]$ represents the final concentration of PH after catalytic hydrogenation reaction.

The HP is calculated with Eq. (3).

$$HP(\%) = \frac{\left(Sel._{(PH2)} \times 2 + Sel._{(PH4)} \times 4 + Sel._{(PH8)} \times 8 + Sel._{(PH14)} \times 14\right)}{14} \times Conv.$$

(3)

$Sel._{(PHx)}$ is the selectivity to the PH hydrogenation products, and $Conv.$ is the PH hydrogenation conversion. Hence, HP represents of hydrogenation degree of PH, which is the percent between the real reaction and the theoretic reaction "PH+7H$_2$ to PH14".
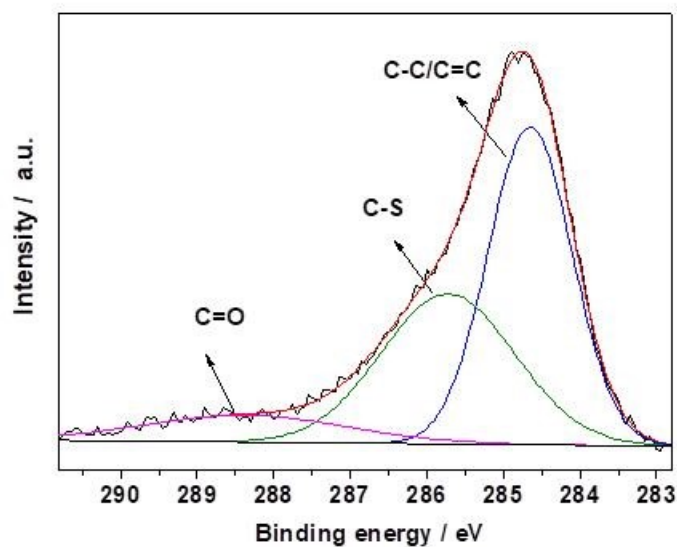
Fig. S1 The C 1s XPS spectrum of MoS_2/C sample.

Three peaks can be observed from the C1s XPS spectrum of MoS_2/C sample in Fig. S1. The binding energy of 284.7 eV can be ascribed to the C-C/C=C bonds in sp2-hybridized carbon.[2-5] The binding energy of 285.8 eV is the C1s peak of typical C-S bond,[4] and the peak at 288.5 eV may be assigned to the C1s peak of C=O bonds.[2] The result of C1s XPS spectrum indicates the successful introduction of C with oxygen functional groups and the interaction between C and MoS_2 in MoS_2/C sample.
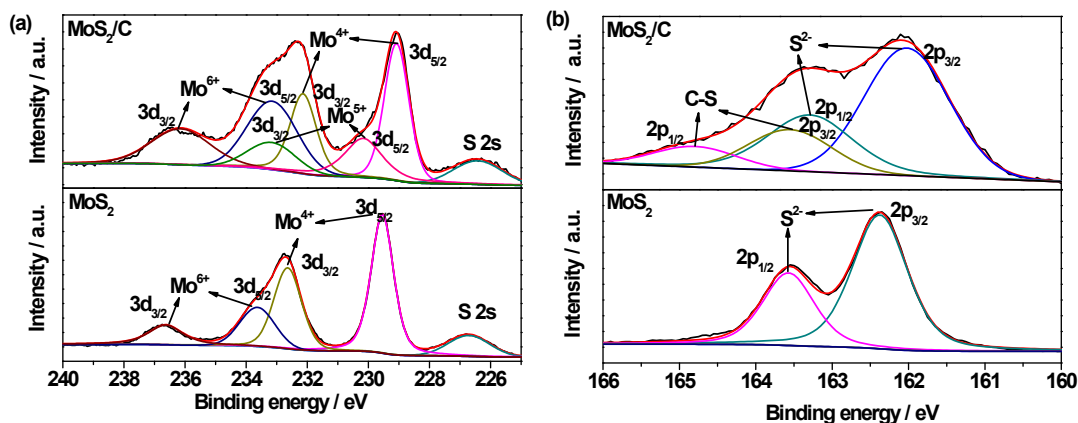
Fig. S2 XPS spectra of (a) Mo 3d, and (b) S 2p for MoS_2 and MoS_2/C samples.

The XPS spectra of Mo 3d and S 2p are given in Fig. S2. As shown in Fig. S2a, the peaks at about 229.5 eV and 232.6 eV can be respectively ascribed to Mo $3d_{5/2}$ and Mo $3d_{3/2}$ of Mo^{4+} in S-Mo-S bonds of MoS_2 sample. For MoS_2/C sample, the peaks at about 229.1 eV (Mo $3d_{5/2}$) and 232.2 eV (Mo $3d_{3/2}$) can be assigned to Mo^{4+} in S-Mo-S bonds in MoS_2/C sample. The binding energies of Mo 3d for MoS_2/C sample shift negatively for 0.4 eV compared with those of MoS_2 sample. Besides, Mo^{5+} and Mo^{6+} can be determined from the Mo 3d XPS spectrum of MoS_2/C sample. However, only Mo^{6+} can be observed in the Mo 3d XPS spectrum of MoS_2 sample. The high-valent Mo may be generated by the intercalated species such as H_2O or C with oxygen functional groups in MoS_2 and MoS_2/C samples.

XPS spectra of S 2p of MoS_2 and MoS_2/C samples in Fig S2b exhibit two binding energies of 162.4 eV and 163.6 eV, which are correspondingly ascribed to S $2p_{3/2}$ and S $2p_{1/2}$ of S^{2-} for MoS_2 sample. The S $2p_{3/2}$ and S $2p_{1/2}$ of S^{2-} can be observed at 161.9 eV and 163.1 eV for MoS_2/C sample in Fig. S2b. The binding energies of S 2p for MoS_2/C sample shift negatively for 0.5 eV in comparison with those of MoS_2 sample. In addition to S^{2-}, the binding energies at 163.4 eV and 164.6 eV can be ascribed to the S $2p_{3/2}$ and S $2p_{1/2}$ of C-S bonds, which proves the self-assembly interaction between C and MoS_2.

We measured the lateral sizes of 177 MoS_2 slabs in 67 MoS_2/C nanosheets for scientific analysis of the layer structure.

The average lateral size $\bar{L}$ of MoS_2 slab was calculated as follows:

$$\bar{L} = \frac{\sum\limits_{i=1...n} l_i}{n} \tag{4}$$

where l_i is the lateral size of MoS_2 slab i, and n is the total number of slabs.

The average stacking layer number $\bar{N}$ of MoS_2 slab was calculated as follows:

$$\bar{N} = \frac{\sum\limits_{i=1...t} n_i \cdot N_i}{\sum\limits_{i=1...t} n_i} \tag{5}$$

where n_i is the number of stacking layers in N_i layers.

MoS_2 dispersion (D) was statistically evaluated by dividing the total number of Mo atoms at the edge surface (M_e) and corner sites (M_c) by the total number of Mo atoms (M_T), [6-8] using the lateral sizes measured in the TEM images:

$$D = \frac{Mo_e + Mo_c}{Mo_T} = \frac{\sum\limits_{i=1...t} 6n_i - 6}{\sum\limits_{i=1...t} 3n_i^2 - 3n_i + 1} \tag{6}$$

where n_i is the number of Mo atoms along one side of the MoS_2 slab, as determined by its lateral size $(L = 3.2(2n_i - 1)[\text{Å}])$, and t is the total number of slabs in the TEM images.

According to Eq. (6), the MoS_2 dispersion (D) is correlated with the average lateral size, and is independent of the average stacking layer number. Rim sites are the active sites of catalytic hydrogenation.[9] The Rim-dispersion (R) for MoS_2 sheets can be deduced according to equation 7. So the R is dependent of both the average lateral size and average stacking layer number.

Stacking layer number ≤ 2

$$R = D$$

Stacking layer number > 2

$$R = \frac{2}{\bar{N}} * D$$
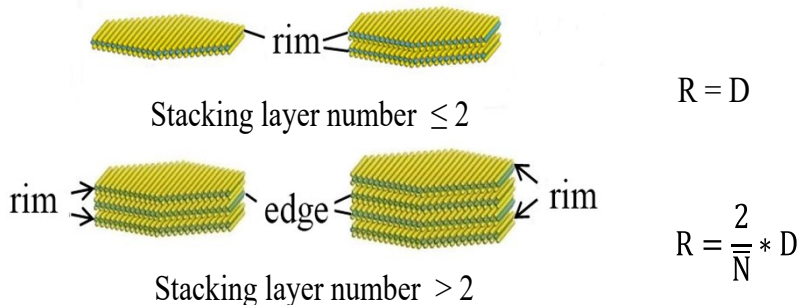
$$\tag{7}$$
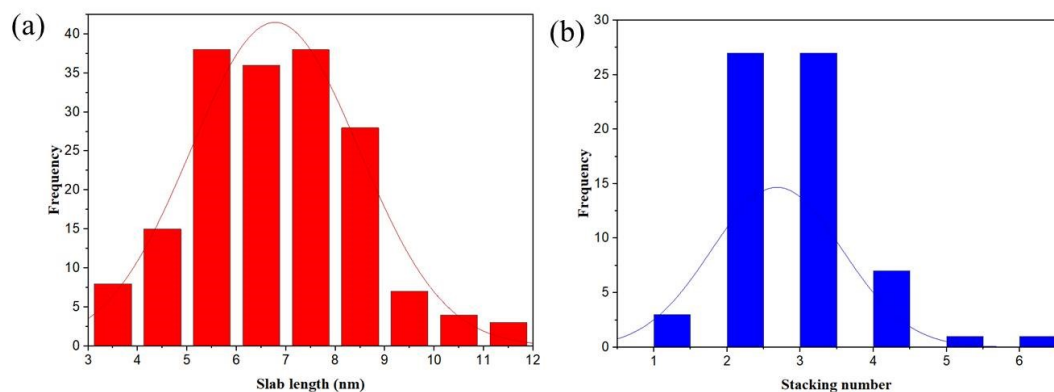
Fig. S3 (a) The lateral size and (b) stacking number distributions of MoS_2 in MoS_2/C nanosheets.
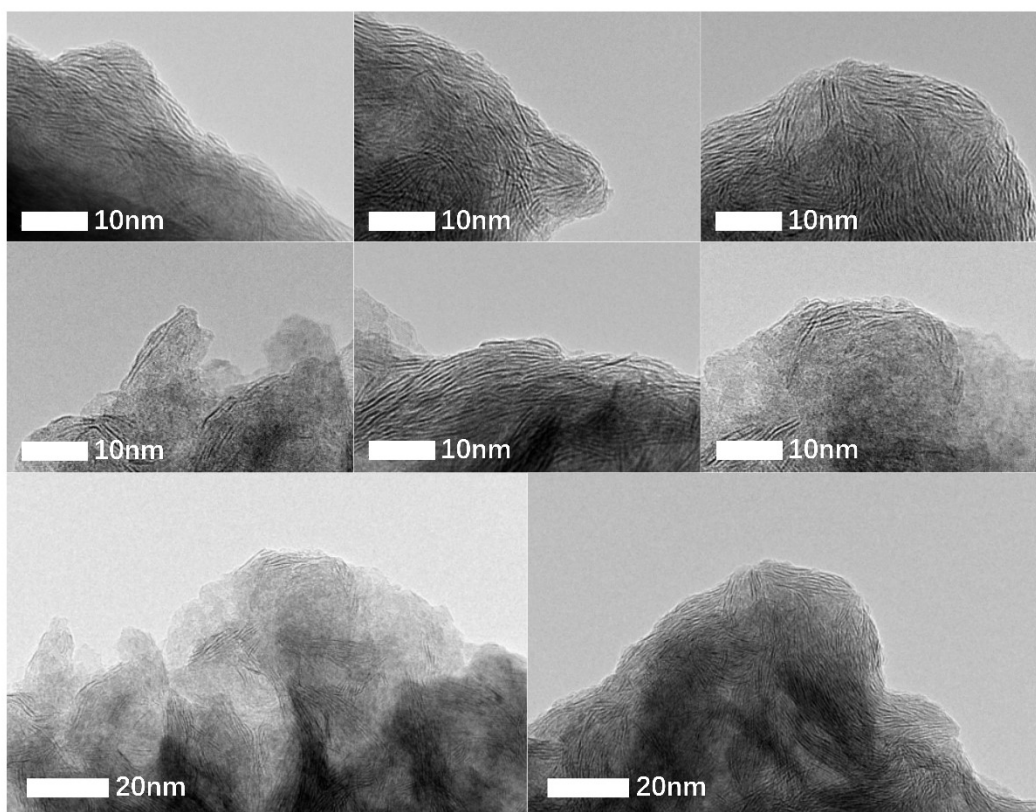
Fig. S4 HRTEM images used to measure the layer structures of MoS_2/C sample.

Fig. S4 shows partial TEM images used to measure the layer structures of MoS_2/C sample. In order to collect statistics data of average stacking layers and lateral sizes, we respectively counted 177 MoS_2 slabs in 67 batches of MoS_2/C nanosheets from

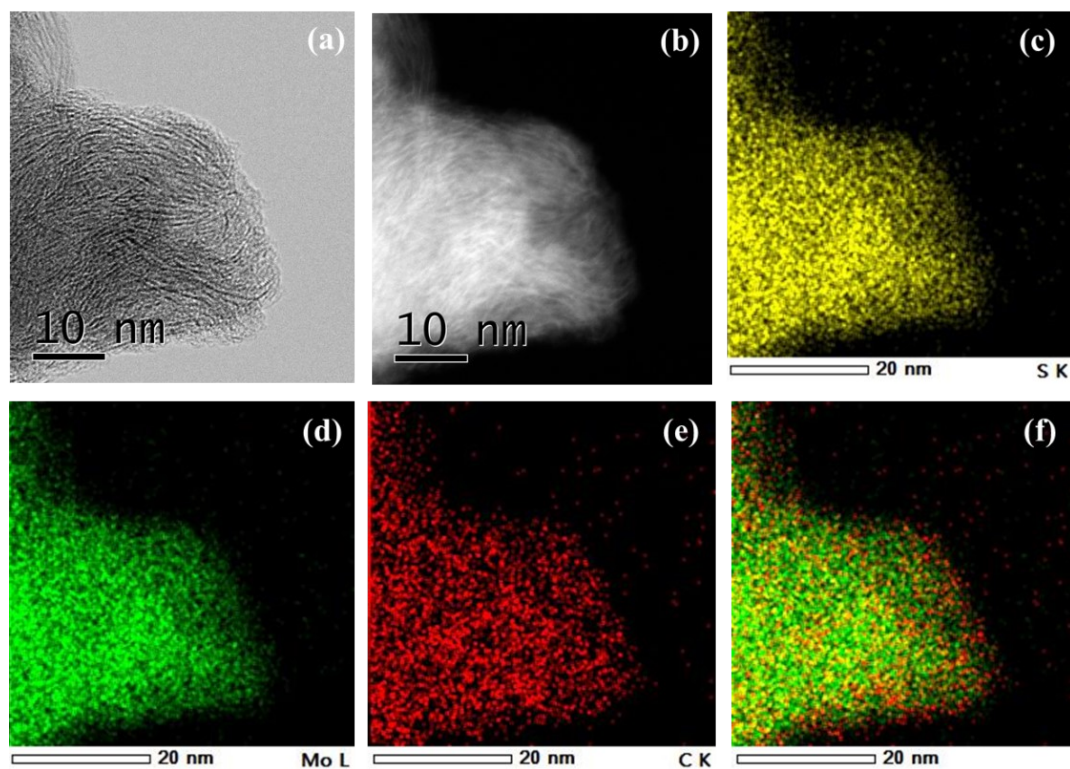more than 10 images obtained by the HRTEM characterization.

Fig S5 The STEM/EDS mapping of MoS_2/C catalyst. (a) Bright field STEM image and (b) Dark field STEM image of MoS_2/C catalyst, (c) S element mapping, (d) Mo element mapping, (e) C element mapping and (f) The mapping overlay of Mo and C elements.

Fig. S5 shows the element mapping of MoS_2/C catalyst. Mo, S and C elements can be detected, and display the analogous distributions in MoS_2/C catalyst. The mapping overlay in Fig.S5f comfirms the uniform distribution of MoS_2 and C in layer-by-layer self-assembly MoS_2/C catalyst.
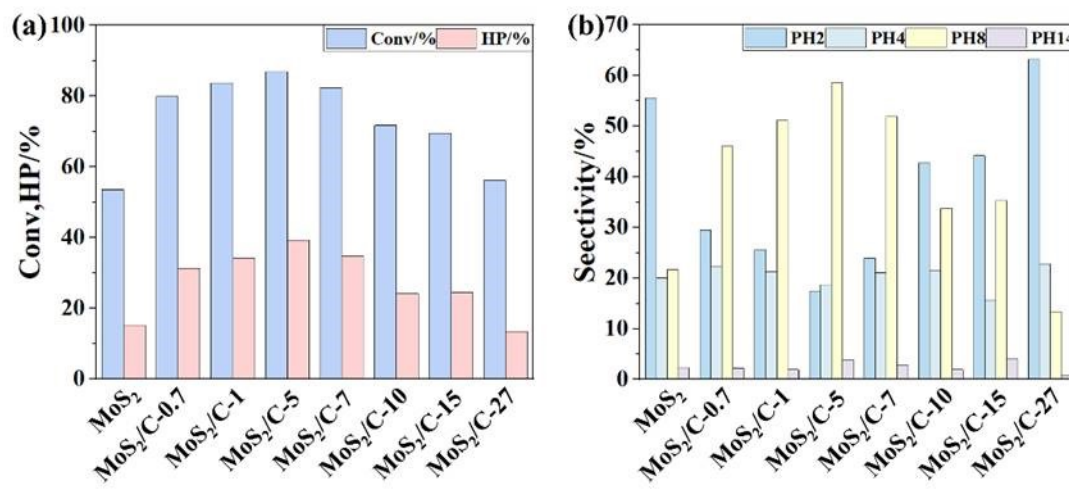
Fig. S6 (a) Conversion (Conv) and hydrogenation percent (HP) of phenanthrene; (b) Selectivity to hydrogenated products (PH2, PH4, PH8 and PH14) of catalytic phenanthrene (PH) hydrogenation with MoS_2 catalyst and MoS_2/C catalysts synthesized with different C/Mo molar ratios in the synthesis medium.

For the catalyst hydrogenation of PH over MoS_2 catalyst, low active catalyst exhibits higher selectivity to preliminary hydrogenation product PH2, lower selectivity to deep hydrogenation product PH8, lower PH conversion and lower hydrogenation percentage. On the contrary, high active catalyst demonstrates lower selectivity to preliminary hydrogenation product PH2, higher selectivity to deep hydrogenation product PH8, higher PH conversion and higher hydrogenation percentage. In this work, the hydrogenation percentage represents the hydrogenation saturation degree of PH, and it is positively correlated with PH conversion and selectivity to deep hydrogenation product.

The catalytic hydrogenation activities of all the MoS_2/C catalysts were evaluated and given in Figure S6. As the C/Mo molar ratio increased in the raw materials from 0.7 to 5, the obtained MoS_2/C catalysts demonstrated enhanced catalytic activities of phenanthrene hydrogenation in comparison with MoS_2 catalyst. When the C/Mo molar ratio is further increased in the raw materials from 5 to 27, the obtained MoS_2/C

catalysts displayed decreased catalytic activities of phenanthrene hydrogenation. Figure S6 indicates that MoS_2/C catalyst synthesized with C/Mo molar ratio of 5 exhibits the highest catalytic activity of phenanthrene hydrogenation.
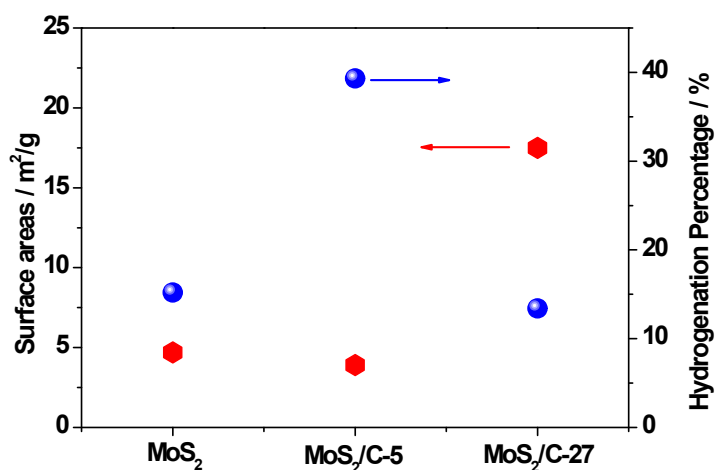

Fig. S7 The surface areas and hydrogenation percentages of MoS_2 and MoS_2/C catalysts.

The surface areas of MoS_2 and MoS_2/C-5 catalysts are respectively 4.7 m^2/g and 3.9 m^2/g, which are very close and smaller than 5.0 m^2/g. Although MoS_2 catalyst has larger particle size than that of MoS_2/C catalyst, the MoS_2 nanosheets in MoS_2 catalyst assembled loosely. Hence the surface area of MoS_2 catalyst is slightly larger than that of MoS_2/C catalyst. The surface area of MoS_2/C-27 synthesized with high C/Mo molar ratio in the precursor is 17.5 m^2/g, which is much higher than those of MoS_2 and MoS_2/C-5 catalysts. However, according to Fig. S7, MoS_2/C-27 with larger surface area exhibits much lower catalytic activity of PH hydrogenation than that of MoS_2/C. Therefore, it can be speculated that catalytic activity for MoS_2 catalyst has no direct correlation with its surface area. The results are consistent with previous reported works.[9-14]

Reference

1. A. Stanislaus, B. H. Cooper, *Catal. Rev. Sci. Eng.,* 1994**, 36**, 75-123.

2. L. Ma, X. Zhou, X. Xu, L. Xu, L. Zhang, W. Chen, *Adv. Powder Technol.,* 2015, **26**, 1273-1280.

3. L. Yang, X. Wang, Y. Liu, Z. Yu, R. Li, J. Qiu, *Catal. Sci. Technol.,* 2017, **7**, 693-702.

4. T. Yao, M. Yao, H. Wang, *Sustain. Energy Fuels,* 2022, **6**, 822-833.

5. F. Xiao, X. Yang, H. Wang, J. Xu, Y. Liu, D. Y. W. Yu, Rogach, A. L., *Adv. Energy Mater.,* 2020, **10**, 2000931.

6. S. Kasztelan, H. Toulhoat, J. Grimblot, J. P. Bonnelle, *Appl. Catal.,* 1984, **13**, 127-159.

7. K. D. Kim, Y. K. Lee, *J. Catal.,* 2019, **369**, 111-121.

8. C. Yang, D. Wang, R. Huang, J. Han, N. Ta, H. Ma, W. Qu, Z. Pan, C. Wang, Z. Tian, , *Chin. J. Catal.,* 2023, **46**, 125-136.

9. D. Wang, J. Li, H. Ma, C. Yang, Z. Pan, W. Qu, Z. Tian, *J. Energy Chem.,* 2021, **63**, 294-304.

10. T. F. Jaramillo, K. P. Jørgensen, J. Bonde, J. H. Nielsen, S. Horch, I. Chorkendorff, *Science,* 2007, **317**, 100-102.

11. P. V. Afanasiev, *C. R. Chimie,* 2008, **11**, 159-182.

12. M. Ramos, G. Berhault, D. A. Ferrer, B. Torres, R. R. Chianelli, *Catal. Sci. Technol.,* 2012, **2**, 164-178.

13. Z. Wu, B. Fang, Z. Wang, C. Wang, Z. Liu, F. Liu, W. Wang, A. Alfantazi, D. Wang, D. P. Wilkinson, *ACS Catal.,* 2013, **3**, 2101-2107.

14. M. Li, D. Wang, J. Li, Z. Pan, H. Ma, Y. Jiang, Z. Tian, A. Lu, *Chin. J. Catal.,* 2017, **38**, 597-606.